Cambridge Centre for Computational Chemical Engineering

University of Cambridge

Department of Chemical Engineering

Preprint ISSN 1473 – 4273

Investigating Cycle to Cycle Variations in an SI Engine Through Experiments and a New Computational Model

Jonathan Etheridge [1] , Sebastian Mosbach [1] , Markus Kraft [1] , Hao Wu [2] ,

Nick Collings [2]

released: 9 December 2008

[1] Department of Chemical Engineering
University of Cambridge
New Museums Site
Pembroke Street
Cambridge, CB2 3RA
UK
E-mail: mk306@cam.ac.uk

[2] Department of Engineering
University of Cambridge
Trumpington Street
Cambridge, CB2 1PZ
UK

Preprint No. 62

c4e

Key words and phrases: SI engine modelling, detailed chemistry, cycle to cycle variation

Edited by
Cambridge Centre for Computational Chemical Engineering
Department of Chemical Engineering
University of Cambridge
Cambridge CB2 3RA
United Kingdom.

Fax: + 44 (0)1223 334796
E-Mail: c4e@cheng.cam.ac.uk
World Wide Web: http://www.cheng.cam.ac.uk/c4e/

Abstract

This paper presents experimental results and a new computational model that investigate Cycle to Cycle Variations (CCVs) in a Spark Ignition (SI) engine. An established Stochastic Reactor Model (SRM) previously used to examine Homogeneous Charge Compression Ignition (HCCI) combustion has been extended by spark initiation, flame propagation and flame termination sub-models in order to simulate combustion in SI engines. The model contains a detailed chemical mechanism but relatively short computation times are achieved. The flame front is assumed to be spherical and centered at the spark location, and a pent roof and piston bowl geometry are accounted for. The model is validated by simulating the pressure profile and emissions from an iso-octane fueled single cylinder research engine that showed low CCVs. The effects of key parameters are investigated. Experimental results that show cycle to cycle fluctuations in a four-cylinder naturally aspirated gasoline fueled SI engine are presented. The model is then coupled with GT-Power, a one-dimensional engine simulation tool, which is used to simulate the breathing events during a multi-cycle simulation. This allows investigation of the cyclic fluctuations in peak pressure. The four cylinder engine has been modified so that transition to HCCI operation is possible via cam profile switching. It is then demonstrated why the detailed exhaust composition obtained may be necessary to simulate the transition between SI-HCCI-SI engine operating modes in future work.

Contents

1 Introduction

Homogeneous Charge Compression Ignition (HCCI) is a promising mode of engine operation for achieving high efficiency and low NO_x and particulate emissions. Unlike Spark Ignition (SI) and Compression Ignition Direct Injection (CIDI) engines, in which combustion is initiated with a spark or fuel injection, there is no direct ignition control in HCCI, where combustion is determined by the chemical kinetics of the mixture. The in-cylinder temperature, pressure and composition at Inlet Valve Closing (IVC) determine the combustion phasing. To accurately model HCCI combustion it is therefore beneficial to use a detailed chemical mechanism. Probability Density Function (PDF) based models have proven advantageous for simulating HCCI combustion due to their ability to incorporate detailed chemistry whilst maintaining low computation times [1].

There are still difficulties in HCCI operation that must be overcome before it can be incorporated into commercially available vehicles. Problems with large heat release rates at high loads have led to the possibility of using a modified SI engine operated in HCCI mode at low to mid loads and switching to SI operation at high loads [2, 3]. To achieve HCCI combustion at compression ratios used in SI engines a Negative Valve Overlap (NVO) can be used to trap exhaust gas in the cylinder, raising the temperature at IVC [4, 5].

The transition from SI to HCCI operation is problematic due to the very different operating conditions, especially when large amounts of exhaust gas from the final SI cycle are used [6–10]. Modelling the transition can help greatly with understanding the overall process, along with independent effects of key parameters that are experimentally difficult to decouple. It is also extremely useful for developing and testing control strategies. A model capable of simulating both operating modes with detailed chemistry is therefore beneficial for understanding the transition.

Combustion in SI engines takes place in a turbulent flow field. The structure and speed of the flame depend on charge motion, composition, temperature and chamber geometry. Detailed SI models exist that predict the structure and propagation of the turbulent flame [11, 12]. To run many cycles of a CFD model with detailed chemistry however would be computationally expensive so has been avoided in this work. Less complex models exist that assume the flame is spherical and propagates at the turbulent flame speed from the spark [13, 14]. In these models the cylinder is divided into unburned and burned zones and the burned zone may be subdivided into several zones that have burned at different times. The burned zone composition is frequently calculated by assuming the mixture behind the flame front reaches equilibrium. However the exhaust gas composition and temperature are important for modelling the transition from SI to HCCI, in which components that do not reach equilibrium, such as NO_x may play an important role.

Cycle to cycle variations (CCVs) in SI engine combustion are a common problem which reduce performance due to variations in combustion phasing, and, in some circumstances,

can lead to knocking or misfire. It is important to understand the variations that can occur in the final cycle before HCCI combustion in order to develop a robust control strategy for the transition between operating modes. Several causes of CCV are known and the magnitude of their effects varies between engine design and operating conditions. In-cylinder charge motion can vary between cycles, altering the rate at which unburned mixture is entrained and the shape of the turbulent flame front. The total mass of fuel, air and EGR can vary between cycles as well as local compositions in the cylinder, which are especially important near the spark location at the time of ignition. Variations in local turbulence at the time of spark can lead to a movement of the flame kernel altering the interactions between the flame and the piston and cylinder walls. Many studies of these effects have been completed. In [15], variations in the peak pressures of two different engines were simulated by random fluctuations, with a normal distribution, in the rms turbulent velocity. Fluctuations in injected fuel mass were also given as a possible cause of the measured CCV. Other experimental work found that CCV is not as dependent on cyclic fluctuations in spray as previously thought and the flow just after time of spark has a greater effect [16]. Convection of the flame kernel has also been investigated and proposed to be a key factor [17, 18]. Movement of the flame kernel and the time delay before the flame becomes fully turbulent have also been discussed in [19] as effects of variations in the rms turbulent velocity.

In this paper we present a new PDF based SI model that uses a detailed chemical mechanism. The model has been created from a previously developed Stochastic Reactor Model (SRM) used to model HCCI combustion so that the transitions between SI-HCCI-SI may be simulated in future work. The model has been validated by simulating a single cylinder research engine which demonstrated low cycle to cycle variation. The model was then coupled with GT-Power, a one-dimensional engine simulation tool, which was used to simulate the breathing events during multi-cycle simulation. Experimental results from a four-cylinder naturally aspirated gasoline fueled SI engine were modelled and the cyclic fluctuations in pressure investigated. Exhaust gas compositions from different SI cycles were then used in HCCI simulations.

The paper is structured as follows. In the next section the model details and implementation is reported. A description of both engine set-ups is given at the start of Section 3. Calibration of the model using experimental data from a single cylinder research engine is then presented. The following section contains results from a sweep of some of the key parameters. Subsequently the model is calibrated using experimental data from fast, slow and average cycles from a four-cylinder engine that can also operate in HCCI mode. Results from a multi-cycle simulation used to model cyclic fluctuations are contained in the same section along with experimental measurements of emissions. This is followed by a demonstration of the effect of exhaust gases from different SI cycles on HCCI combustion. Finally conclusions are drawn and future work outlined.

2 Model Details

The model was built into the framework of the SRM used to simulate HCCI combustion [1, 20–22]. The SRM is based on the PDF transport equation and models convective heat transfer, turbulent mixing, piston movement and detailed chemistry. The PDF is approximated by dividing the charge into a notional ensemble of N_{Tot} stochastic particles.

For SI simulation the particle ensemble is divided into three zones: unburned, entrained and burned. Mixing occurs within each zone but not between zones and all particles are initially in the unburned zone. The Euclidean Minimum Spanning Tree (EMST) mixing model was used in each zone and is described in [23]. The entrained zone is subdivided into unburned and burning particle categories to keep track of the particles' states as will be discussed later. Chemistry occurs at every CAD step in every particle as in the HCCI model. The PRF mechanism used contains 157 species and 1552 reactions. The model could be used to investigate knocking as in [24, 25], however similar work is not presented here. The main SRM operator splitting loop, with the addition of spark initiation, flame propagation and flame termination was implemented as follows:

1. Initialize $t = 0$, Δt, CAD = IVC, CAD_{spark}, spark energy, $R_f = 0$, $N_U = N_{Tot}$, $N_E = N_B = 0$ all particles are in the unburned zone. Determine temperature, composition, mass, volume and pressure of particle ensemble.
2. Progress in time $t \mapsto t + \Delta t$. If CAD $\geq$ EVO or $t \geq t_{stop}$ then save the detailed exhaust composition as input EGR and stop.
3. Perform volume change due to piston movement.
4. Perform the mixing step.
5. Perform stochastic heat transfer.
6. Perform the pressure equilibration step.
7. If CAD $\geq \text{CAD}_{spark}$ and $N_U = N_{Tot}$ perform spark initiation (as described below) else if CAD $\geq \text{CAD}_{spark}$ and $N_U > 0$ perform flame propagation (as described below) else go to (8).
8. Perform the chemistry step. If $N_E > 0$ perform flame termination (as described below).
9. Perform the pressure equilibration step.
10. Perform the mixing step.
11. Go to step (2).

2.1 Spark Initiation

The diameter of the entrained zone at the time of spark was set to 1.0 mm, the rough size of the spark gap. The first particle randomly chosen to enter the entrained zone is not added all at once but the actual entrained volume is removed from it and added to a new particle in the entrained zone. If the energy in the spark were to be distributed uniformly throughout a volume represented by a particle, then the temperature would not be sufficient to initiate combustion. Once the entrained volume has increased above the particle's volume, it is reunited into a single particle. The spark is simulated by setting the temperature of the mass added to the entrained zone at each step to 2000 K, until all of the spark energy has been added. This low temperature was chosen to prevent any problems with the chemical mechanism, which was not developed to represent the high temperatures experienced at the spark, which have been estimated to be of the order 60,000 K [26]. The spark initiation was modelled as follows:

1. If $N_E > 0$ go to (7) else go to (2).
2. Set the flame radius to R_f = 0.5 mm.
3. Select a particle at random with a uniform distribution.
4. Remove the spherical volume with 0.5 mm radius from the particle and add to a newly created particle in the entrained zone. N_E = 1, $V^E = 4/3\pi R_f^3$.
5. Increase the temperature of the entrained particle to 2000 K by adding energy at constant pressure. Remove the energy added from the input spark energy.
6. Go to the chemistry step.
7. Calculate the new flame volume, V_f, as described in the flame propagation section.
8. If $V_f > V^U_{Next} + V^E$ go to (13) else go to (9).
9. Remove V_f - V^E from the unburned particle being entrained.
10. If there is spark energy remaining, increase the temperature of the freshly entrained mass to a maximum of 2000 K by adding energy at constant pressure.
11. Reunite the freshly entrained mass with the entrained particle.
12. Go to the chemistry step.
13. Remove the unburned particle being entrained from the unburned zone, $N_U = N_{Tot}$ - 1.
14. If there is spark energy remaining, increase the temperature of the freshly entrained mass to a maximum of 2000 K by adding energy at constant pressure.
15. Reunite the freshly entrained mass with the entrained particle.
16. Select the next particle to entrain, at random with a uniform distribution. Go to step (2) in flame propagation section described below.

2.2 Flame Propagation

A randomly chosen particle is moved from the unburned zone to the entrained zone when the calculated flame volume exceeds the burned and entrained zone volumes by more than half the volume of the next particle to be entrained. The volume of the flame is calculated from the geometry of the piston and cylinder, and the flame radius assuming it is spherical and centred at the spark location. The flame radius at the n^{th} time step, $R_{f;n}$, is obtained from

$$R_{f;n} = R_{f;n-1} + \left(u_T \left(1 - \exp\left(\frac{-(t - t_{spark})}{\tau_b} \right) \right) + S_L \right) \Delta t. \tag{1}$$

The increase in flame radius is calculated as the time step multiplied by the entrainment velocity. The radius initially increases at the laminar flame speed, S_L,until a wrinkled turbulent flame front develops after a characteristic burn time, τ_b [26, 27]. The characteristic burn time is given by

$$\tau_b = \frac{l_T}{S_L}, \tag{2}$$

where l_T is the characteristic length scale [26].

The mixing time in the entrained zone, τ_E, is increased at the same exponential rate as the transition from a laminar to a turbulent flame. The mixing time increases to the value τ_E^{max} once the turbulent flame has fully developed. Before this the entrained zone mixing time is smaller causing faster mixing and heat release. This was included as the rate of burning is initially the rate of entrainment before a turbulent flame front has developed containing unburned pockets [19].

$$\tau_E = \tau_E^{max} \left(1 - \exp\left(\frac{-(t - t_{spark})}{\tau_b} \right) \right) \tag{3}$$

The rate of burning is controlled by the mass entrained and the rate it mixes with the hot, reacting entrained material and is calculated with the detailed chemical mechanism. The maximum entrained zone mixing time was set around ten times smaller than the other zones to prevent the volume of the entrained zone growing unrealistically large and to propagate heat through the entrained zone at the correct rate. Flame propagation was implemented in the model as follows:

1. Increase the flame radius using equation (1) and calculate the new flame volume, V_f.
2. Update the entrained zone mixing time according to equation (3).
3. If $\mathrm{V}_f > \sum_{i=1}^{N_E} V_i^E + \sum_{i=1}^{N_B} V_i^B + 1/2\mathrm{V}_{Next}^U$ go to (4) else go to (6).
4. Add the particle to the entrained zone and select the next particle to be added randomly with a uniform distribution. N_U = N_U - 1, N_E = N_E + 1. Flag the newly entrained particle as unburned and entrained.

5. Go to step (3).

6. Perform the chemistry step.

The correlation used to obtain the characteristic flame speed, u_T, was taken from [28]:

$$u_T = 0.08 C_1 \bar{u}_i \left(\frac{\rho_u}{\rho_i} \right)^{1/2}, \tag{4}$$

where $\bar{u}_i$ is the mean inlet gas speed, ρ_u is the unburned gas density and ρ_i is the inlet air density. The correlation used is relatively old, however this work was focused on producing a detailed chemistry SI model incorporated into the SRM to enable the SI-HCCI transition to be simulated at low computational cost. There were no measurements of in-cylinder turbulence, hence the constant C_1 was used to fit the model to the experimental data by varying the rate of entrainment. The model was intended to predict not only the pressure profile, but also temperature and composition so that the transition between SI-HCCI can be simulated.

The cylinder geometry model contains a pent roof and the piston contains a bowl. The volume of the spherical flame is calculated exactly in the bowl and cylinder areas. In the pent roof region numerical integration of the flame cross sectional area at different heights is used to obtain the flame volume.

2.3 Flame Termination

In this section we describe how particles are moved from the entrained zone to the burned zone. During the chemistry step the rate of heat release in each entrained particle is calculated. When the heat release rate of an entrained particle has risen above the heat release rate limit, HRR_{lim}, the particle is classified as entrained and burning. The entrained and burning particles are removed from the entrained zone and added to the burned zone once their heat release rate drops below HRR_{lim}. Particles are also transferred from the entrained zone to the burned zone if they remain in the entrained zone for the maximum length of time, t_E^{max}. This was included in the model to prevent particles that do not reach the heat release rate limit from remaining in the entrained zone throughout the simulation. This will be important if the model is used for a stratified lean burn SI engine as some particles may contain little or no fuel. When no particles remain in the unburned zone, the entrained zone mixing time is set to τ_E^{max} as equation (2) can no longer be evaluated. Flame termination was modelled as follows:

1. If any unburned entrained particle's heat release has risen above HRR_{lim} flag the particle as entrained and burning.

2. If any entrained and burning particle's heat release has dropped below HRR_{lim} move the particle to the burned zone. $N_E = N_E - 1$, $N_B = N_B + 1$.

3. If any entrained particle has spent longer than t_E^{max} in the entrained zone then move it to the burned zone. $N_E = N_E - 1$, $N_B = N_B + 1$.

4. If $N_U = 0$ then $\tau_E = \tau_E^{max}$.

In summary, an SI model has been integrated into the SRM. The particle ensemble is divided into three zones: unburned, entrained and burned. Mixing occurs within each zone but not between zones. Chemistry occurs at every CAD step in every particle as in the HCCI model. An initial temperature and flame radius of 2000 K and 0.5 mm are set at the spark timing respectively. The flame radius is updated using an entrainment velocity. The flame radius and cylinder and piston geometry are used to obtain the flame volume. Particles are moved from the unburned zone to the entrained zone when the calculated flame volume exceeds the burned and entrained zone volumes by more than half the volume of the next particle to be entrained. Particles are removed from the entrained zone and added to the burned zone once their heat release rate has risen above and then drops below HRR_{lim} or if they remain in the entrained zone for t_E^{max} s.

3 Results and Discussion

In this section we present and compare experimental and simulation results from two different engines: a single-cylinder naturally aspirated direct injection iso-octane fueled research engine and a four-cylinder naturally aspirated GDI engine. The engine specifications and operating conditions are given in Table 1.

Table 1: *SI mode engine specifications and operating conditions.*

Engine	Research	SI-HCCI
Cylinders	1	4
Fuel	iso-octane	95 RON gasoline
Bore [mm]	89.0	87.5
Stroke [mm]	90.3	83.0
Con. rod length [mm]	148.9	146.3
Disp. volume [cm^3/cyl]	562	499
CR	11	12
Speed [RPM]	1500	1500
Air/fuel equiv. ratio	1.0	1.0
EGR [%]	15.0	28.8
Spark timing [CAD BTDC]	35	40
Start of Injection [CAD BTDC]	280	308
Inlet valve opening (IVO) [CAD BTDC]	336	392
Inlet valve closing (IVC) [CAD BTDC]	86	82
Exh. valve opening (EVO) [CAD ATDC]	116	139
Exh. valve closing (EVC) [CAD ATDC]	366	449

Exhaust emissions of CO and UHC as well as the in-cylinder pressure were measured in the single-cylinder research engine. The CO volume fraction was measured with a Non-Dispersive Infrared (NDIR) sensor. UHC were measured 200mm downstream of the exhaust valve with a fast Flame Ionisation Detector (FID).

The four-cylinder GDI SI engine was modified to enable it to run in HCCI mode with NVO via cam profile switching. Details of the HCCI mode operating condition are given later. The pressure in each cylinder was monitored with Kistler 6123 piezoelectric transducers and recorded. Emissions of NO_x, CO and UHC were measured using a Horiba EXSA-1500 analyser. More details of the engine can be found in [29].

3.1 Model Calibration

The model was initially calibrated using results from the single cylinder research engine. As fuel injection occurred early during intake, the cylinder charge was assumed to be initially homogeneous in terms of composition and temperature, hence all particles were set to be identical at IVC. The model was calibrated to find values for C_1, τ_E^{max}, t_E^{max} and HRR_{lim}. The values of these parameters are given in Table 2. The pressure profile was matched to the experimental data shown in Figure 1. The emissions matched experimental data reasonably well as shown in Table 3. The model contains a crevice but no wall impingement sub-model, which could be the cause of low UHC emissions. The assumption of homogeneity at IVC could also have contributed to the low emission prediction.

Table 2: *Parameters used in simulation of single cylinder research engine.*

No. Particles	100
CAD step [CAD]	0.2
C_1	10.0
τ_E^{max} [ms]	4.25×10^{-1}
HRR_{lim} [J/kg.s]	1.0×10^9
t_E^{max} [ms]	1.5

Table 3: *Emission results for single cylinder research engine.*

	Exp.	Sim.
UHC [ppm]	600	239
CO [ppm]	2700	2541
NO_x [ppm]	-	886

Figure 2 shows the majority of particles remained in the entrained zone for between 0-1.5 ms when t_E^{max} was not used. The PDF was obtained by taking each value from the

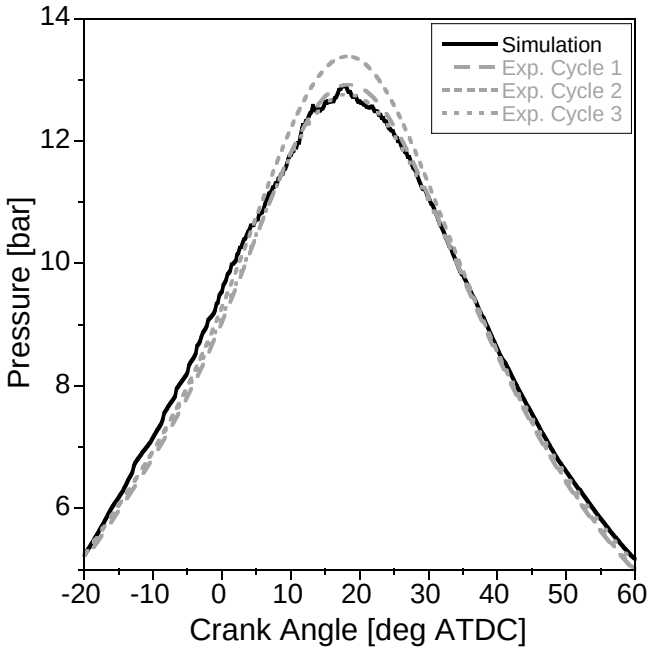

Figure 1: *Comparison of experimental and simulated pressure profiles for the single cylinder research engine.*

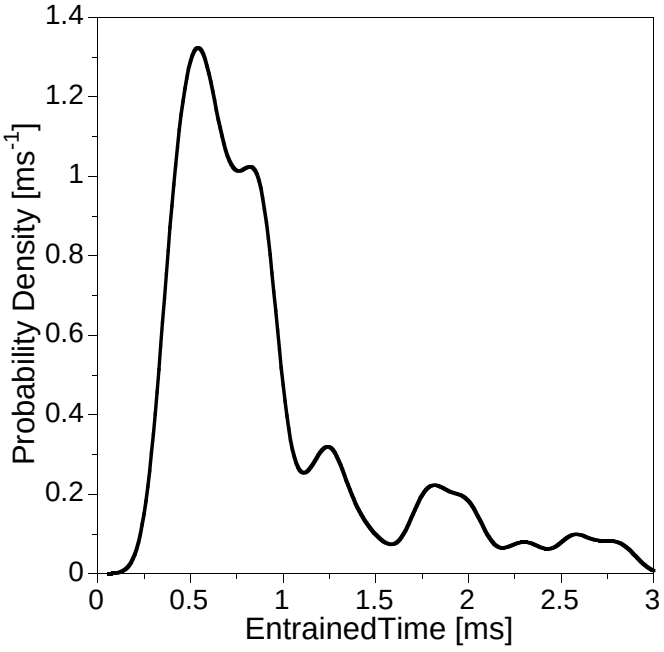

Figure 2: *Probability density of time in the entrained zone when t_E^{max} was not used.*

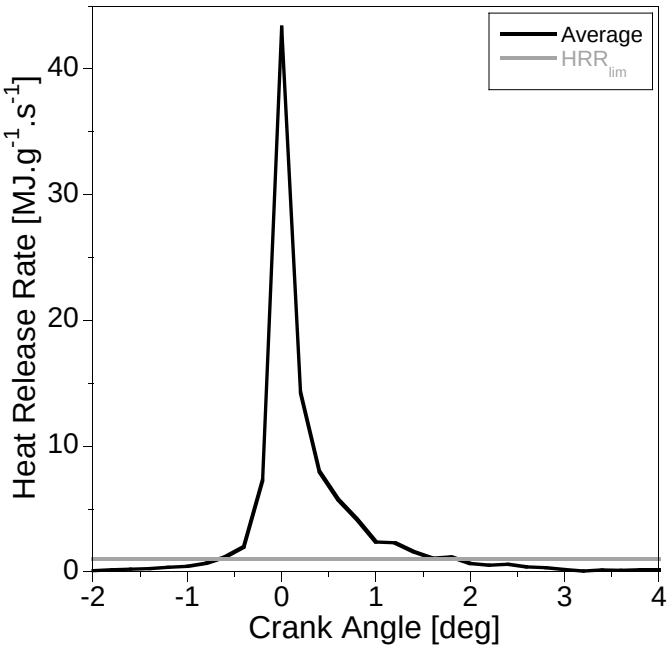

Figure 3: *Average rate of heat release from each particle against CAD, normalised so that all peak rates were at 0 CAD.*

ensemble as the mean of a normal distribution with a σ of 0.08 ms, summing the distributions and dividing by the total number. Introducing this time limit caused a second smaller peak at 1.5 ms as will be seen in later figures. Eight out of the hundred particles reached the entrainment time limit. From experimental observations, the burn time in the turbulent flame front has been estimated at values ranging from 1.0-1.8 ms [19]. Including the time limit had a small effect on the pressure profile and increased the UHC and CO emissions.

Figure 3 shows the average rate of heat release against CAD, calculated by centering each particles' peak heat release rate at 0 CAD and averaging over the 100 particles. The rate of heat release increased rapidly and the majority of the chemical energy was released within 2 CAD. The effect of varying HRR_{lim} will be presented and discussed in the next section.

The number of particles entrained and burning remains roughly constant however the number of particles entrained and unburned grows and then falls off (see Figure 4a). This indicates a thickening flame brush followed by consumption of the remaining fuel as the flame reaches the walls. The temperatures remain roughly constant throughout (see Figure 4b). The unburned entrained region is slightly warmer than the unburned zone due to some particles having mixed with the burning entrained particles. The burning entrained particles are slightly cooler than the burned particles as all the chemical energy has not been released in this zone and particles can mix with the cooler unburned entrained particles.

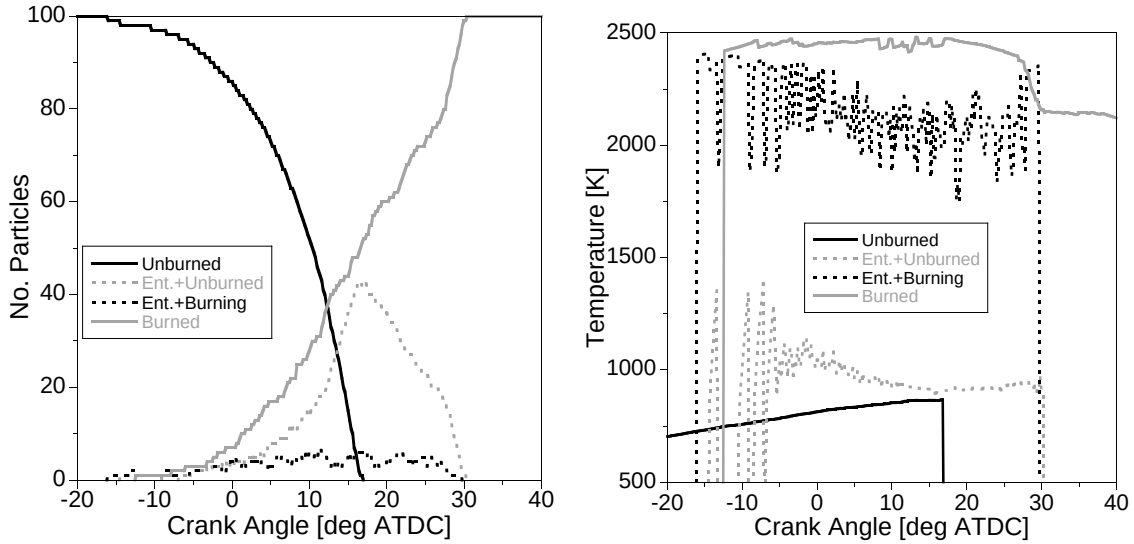

(a) (b)

Figure 4: *Number of particles and the average temperature of each zone against CAD. The entrained zone is split into particles that are releasing more and less than HRR_{lim}, labeled Entrained+Burning and Entrained+Unburned respectively.*

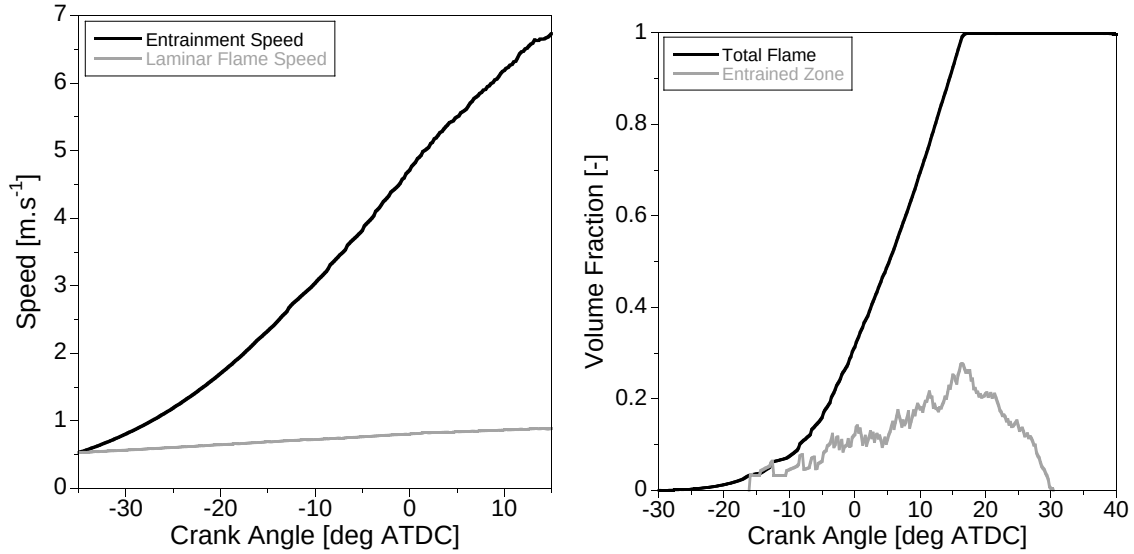

(a) (b)

Figure 5: *Total entrainment and laminar flame speeds and total flame and entrained zone volumes fractions against CAD.*

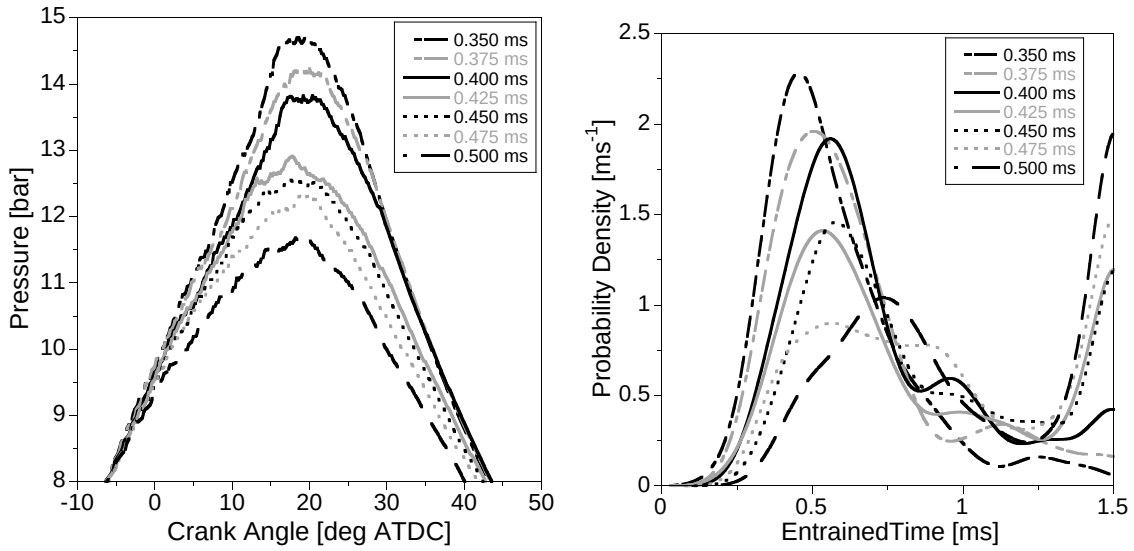

(a) (b)

Figure 6: *Comparison of pressure profiles and entrained time probability density at different values of* τ_E^{max}.

The entrainment speed increases with time due to the increasing pressure and the flame front becoming more wrinkled. The effect of turbulence on the flame front causes the surface area to increase and the rate of mass entrained to rise as can be seen by comparing the laminar flame speed with the entrainment speed in Figure 5a. The laminar flame speed increases due to the temperature rise having a greater effect than the increase in pressure. The total flame volume fraction presented in Figure 5b includes the entrained zone volume fraction. The volume fraction of the cylinder containing the flame only increases linearly with time due to flame contact with the cylinder and piston preventing growth in all directions.

3.2 Parameter Sweeps

In this section we present results from varying key parameters to further validate the model. When particles are added to the entrained zone they do not begin to release large amounts of chemical energy until they mix with hot burning particles (unless knocking occurs). The rate at which this occurs depends on the entrained zone mixing time. Figure 6a demonstrates how increasing the rate of mixing in the entrained zone increases the rate of heat release, causing an increase in the peak pressure. The residence time of particles in the entrained zone decreases as they mix and burn within a shorter time of being entrained (see Figure 6b).

The rate of heat release that determined when a particle was moved from the entrained to the burned zone was varied. Figure 7a shows that reducing HRR_{lim} causes an advance in combustion phasing. This was because the particles release more of their chemical en-

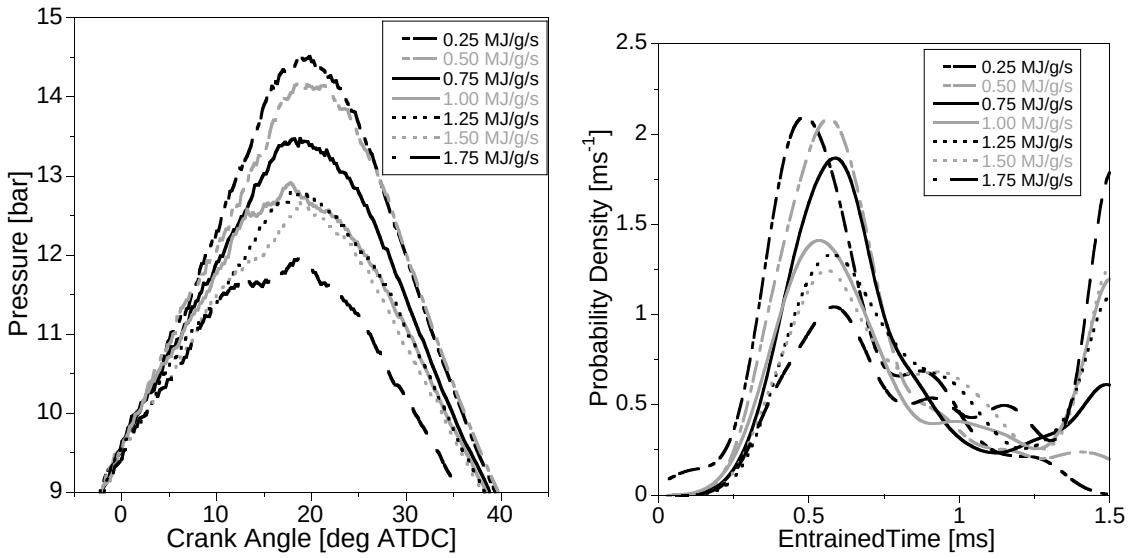

(a) (b)

Figure 7: *Comparison of pressure profiles and entrained time probability density when different heat release rate limits, HRR_{lim}, were used.*

ergy whilst in the entrained zone causing an increase in the zones' temperature. Figure 7b shows the average particle residence time in the entrained zone decreases as HRR_{lim} is reduced. Although the particles are not moved to the burned zone until their heat release rate drops below a lower value, the increased entrained zone temperature causes them to release their chemical energy at a faster rate. If HRR_{lim} is set too high, not enough chemical energy will be released in the entrained zone and the temperature will decrease which could cause the flame to extinguish. The 1.75 MJ/g/s case appears to have been partially quenched because of this. If HRR_{lim} is set too low, then particles that have almost fully burned can mix with unburned particles. The EMST mixing model does however account for localness and will preferentially mix particles with similar compositions.

A spark temperature of 2000 K was chosen as the mechanism was not created for extremely high combustion temperatures that are reached at a spark plug. Figures 8a and 8b suggest this is an acceptable approach as there does not appear to be a trend between the spark temperature and the combustion profile or time spent in the entrained zone at the conditions investigated.

Figure 9a shows that increasing the initial flame radius caused a slight advance in combustion. The effect is not significant given the relatively large range investigated. The peak pressure and time spent in the entrained zone show no correlation at the flame radii investigated (see Figures 9a and 9b). As variations in this parameter caused minor changes in the pressure profile, the initial flame radius assumption was taken as acceptable and a detailed spark initiation sub-model was not implemented.

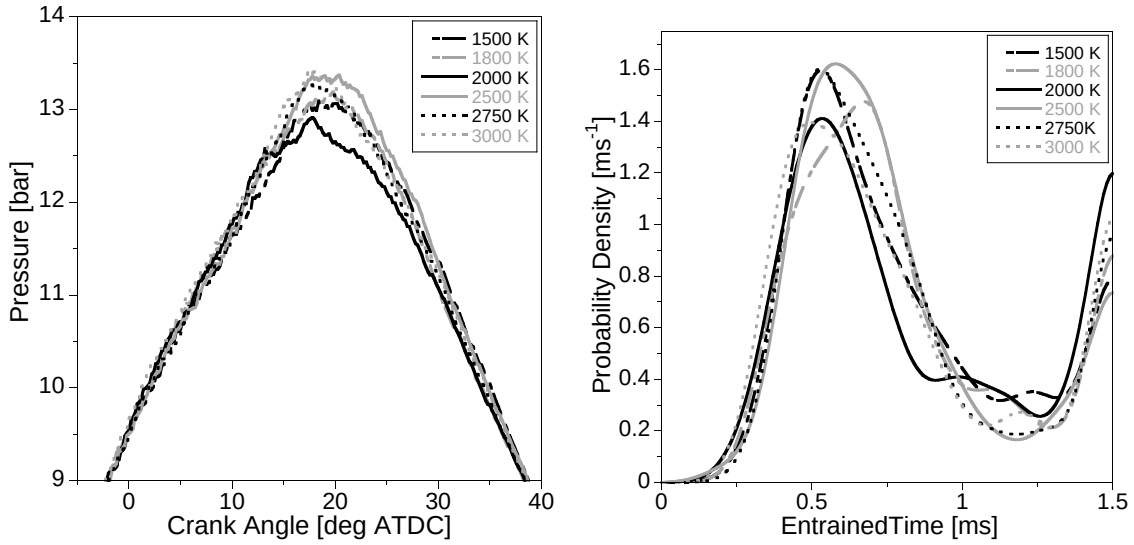

(a) (b)

Figure 8: *Comparison of pressure profiles and entrained time probability density with different spark temperatures.*

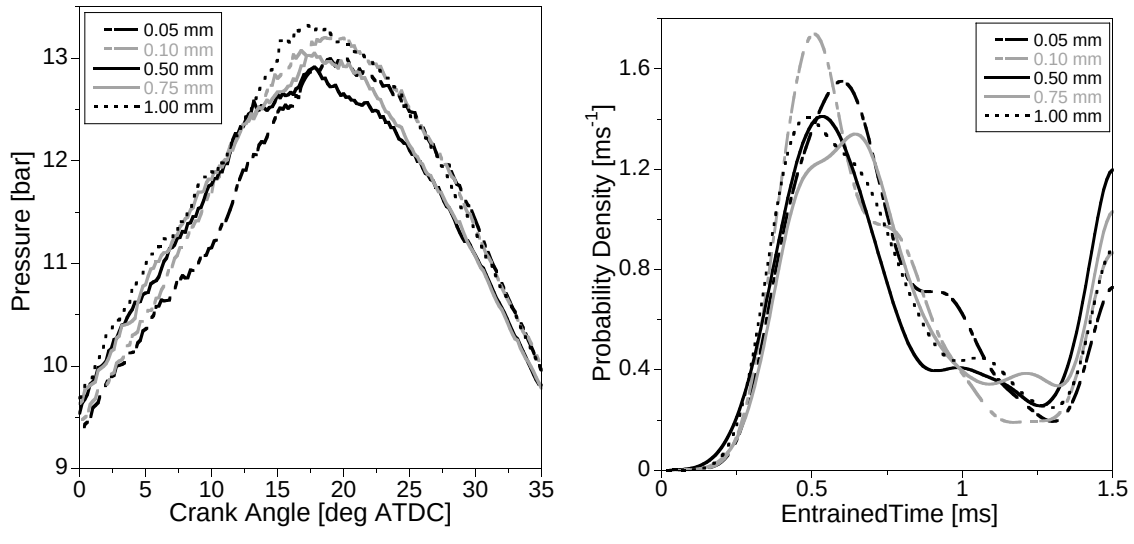

(a) (b)

Figure 9: *Comparison of pressure profiles and entrained time probability density with different initial flame radii.*

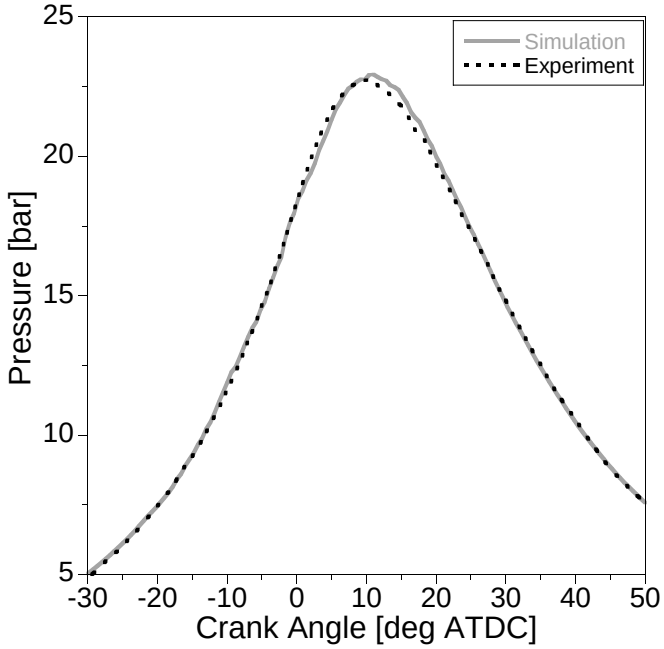

Figure 10: *Comparison between an experimental cycle with an average peak pressure and the simulation.*

3.3 Multi-cycle simulation with CCV

A four-cylinder SI engine modified to operate in HCCI mode at mid loads showed CCV in SI mode at the speed and load investigated. Details of the engine are given in Table 1. Large amounts of internal EGR have been reported to increase CCV [26]. A mixture of 95 % iso-octane and 5 % n-heptane was used to simulate the 95 RON gasoline. The model was calibrated to fit a medium cycle pressure trace from the experimental data which is shown in Figure 10. The model parameters used are given in Table 4.

Table 4: *Parameters used in simulation of SI-HCCI engine.*

C_1	18.0
τ_E^{max} [ms]	7.5×10^{-1}
HRR_{lim} [J/kg.s]	1.0×10^9
t_E^{max} [ms]	1.5

The entrained zone mixing time was varied to see if the fluctuations could be matched. In Figure 11 the results from varying the entrained zone mixing time are presented. Three experimental pressure profiles representing fast, medium and slow burning cycles are shown. The range of peak pressures observed can be re-produced however the phasing does not match the experimental data well. When 1.0 ms was used as τ_E^{max}, the flame appears to have been quenched late on in the cycle. This value varies the simulated turbulence in the

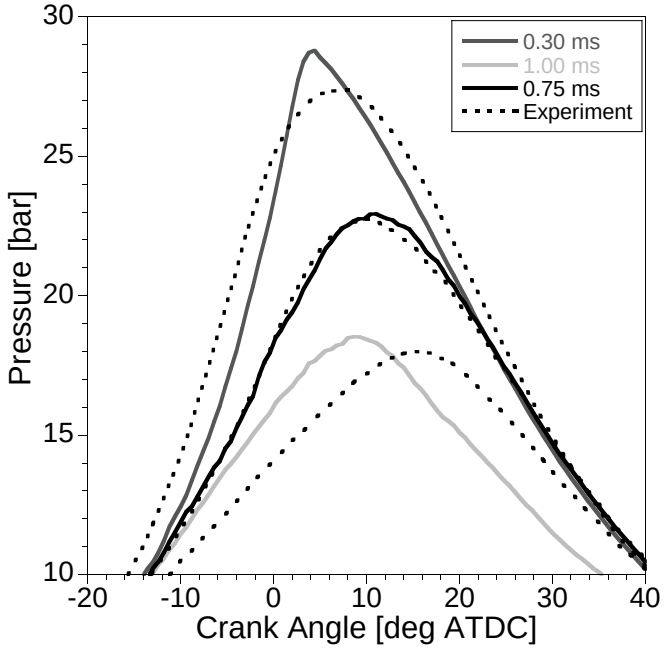

Figure 11: *Fast medium and slow cycles obtained by varying τ_E^{max} compared with experiment.*

entrained zone. It may be necessary to increase C_1 at the same time as decreasing τ_E^{max} as the flame surface area is likely to increase with increased turbulence, hence the rate of entrainment should also increase.

Figure 12 shows experimental pressure against crank angle and the simulation results when C_1 was varied and τ_E^{max} was constant. The pressure traces match the experimental data well with C_1 values of 12 and 35 used to match the slow and fast pressure traces respectively. The cycles in which the flame initially entrains mass at a faster rate, continue to entrain mass at a fast rate throughout the cycle. This suggests variations in the flame surface area occur early in the cycle resulting in different rates of unburned gas entrainment and combustion. This could be caused by the flame kernel being convected towards a wall, reducing the available area, or due to turbulence altering the shape of the kernel early in the cycle resulting in a higher surface area.

Figure 13 shows the PDF of peak pressure obtained from the experimental data and a normal distribution fitted to the data. The peak pressures measured in the experiment fit a normal distribution well. Using the values from the C_1 sweep, a relationship between peak pressure, in bar, and C_1 was obtained for the SI-HCCI engine. Figure 14 shows C_1 against peak pressure in the cylinder and the curve with equation (5).

$$C_1 = 0.024{P_{max}}^3 - 1.4973{P_{max}}^2 + 32.189P_{max} - 221.92. \tag{5}$$

The engine model was coupled with GT-Power, a one dimensional engine simulation tool.

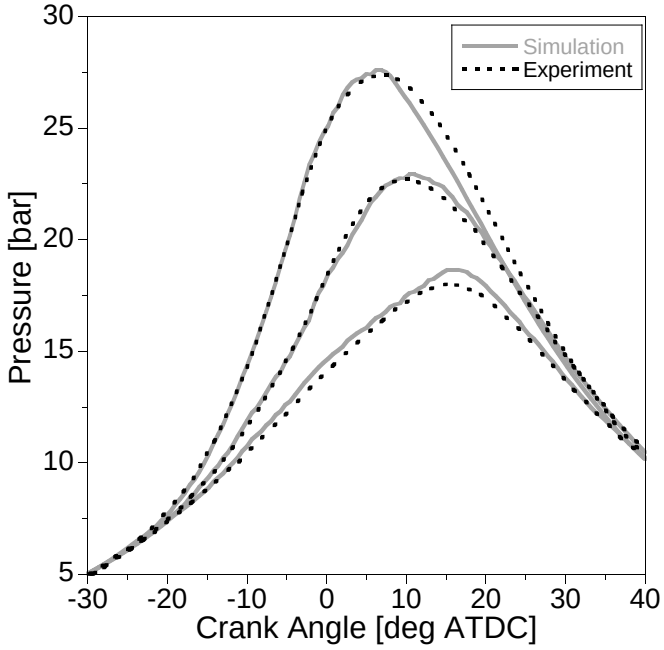

Figure 12: *Fast medium and slow cycles obtained by varying C_1 compared with experiment.*

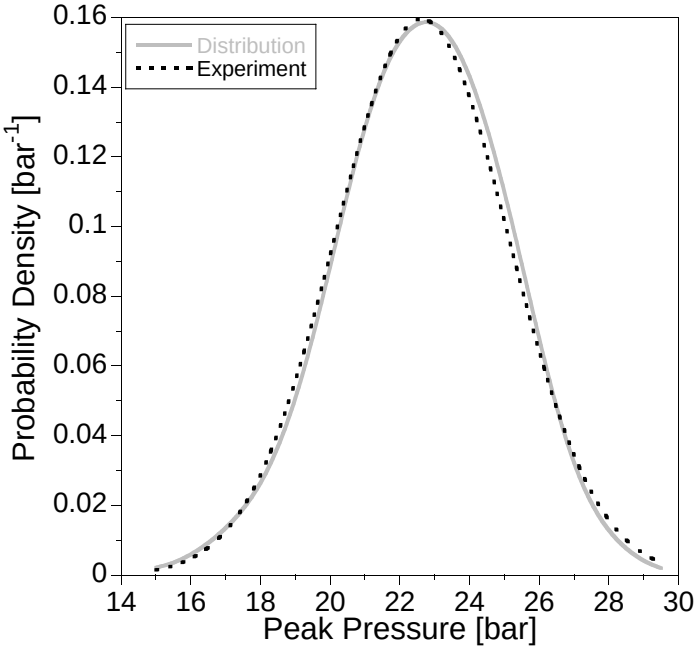

Figure 13: *Normal distribution fit to experimental distribution of peak pressures.*

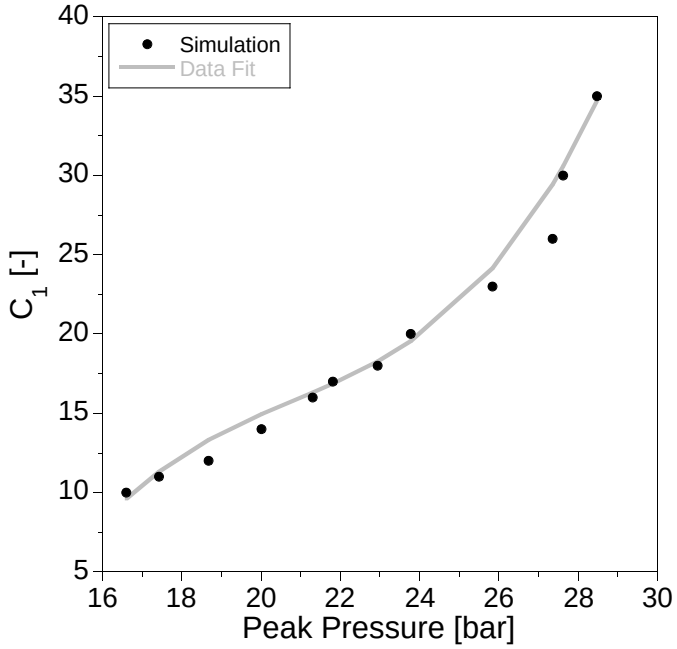

Figure 14: *C_1 against simulated peak pressure.*

The fitted normal distribution of the experimental peak pressures, with mean 22.6 bar and standard deviation 5 bar, was used to generate a random peak pressure for each simulated cycle. The peak pressure was used to obtain C_1 for the cycle using equation (5). The detailed exhaust gas composition was stored at the end of each cycle and used in the following cycle. Forty cycles were simulated and the values of peak pressure against the crank angle they occurred are plotted in Figure 15 along with the experimental results. The simulation matches the experimental data well and the peak pressures do not fall on a straight line but a range of peak pressures were obtained at the same crank angle. This was because the temperature, pressure and composition are all affected by the previous cycle.

Table 5: *Emission results for SI-HCCI engine.*

	Exp.	Sim.
NO_x [ppm]	528	496
UHC [ppm]	3113	115
CO [ppm]	4772	1627

The simulated NO_x emissions reproduced the experimental result well (see Table 5), suggesting the temperatures and the length of time particles spent in each zone were close to that in the experiment. Figure 16 shows the variation in NO_x emissions from cycles with different peak pressures. The faster burning cycles with higher peak pressures produced higher NO_x emissions. The emissions increased almost linearly with peak pressure. This

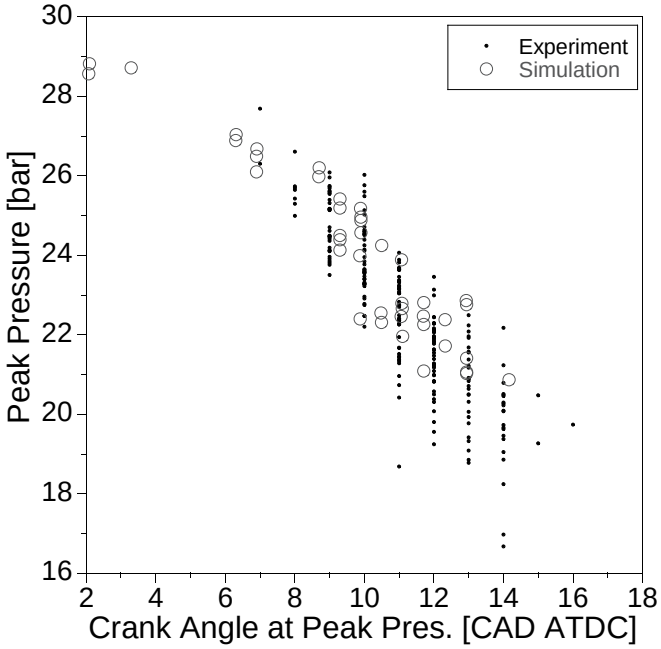

Figure 15: *Peak pressures against crank angle they occurred in 40 simulated and 200 experimental cycles.*

was caused by increased peak combustion temperatures as was expected.

Experimental UHC and CO were higher than the simulated values given in Table 5. This could be due to wall impingement or rich areas in the cylinder that are neglected by the initial assumption of homogeneity. Figure 17a compares CO emissions and the peak pressures during the cycles they occurred over the forty simulated cycles. The same trend was produced by UHC emissions shown in Figure 17b. When peak pressures above 23 bar were reached, the UHC and CO emissions were centered around 1000 ppm and 30 ppm respectively with low variation between cycles. Cycles with peak pressures below 23 bar produced values of the order 1750 ppm and 225 ppm of CO and UHC respectively and exhibited larger fluctuations. This was caused by lower temperatures in the entrained zone, increasing the time particles were flagged as unburned and entrained, increasing particles' residence time in the zone. Particles were then more frequently moved to the burned zone due to spending t_E^{max} s in the entrained zone. Similar trends have been reported in the literature with slower burning cycles producing higher UHC emissions [26]. Figure 18a compares the heat release in the fast and slow simulated cycles shown in Figure 12. Although heat release occurred later in the slow cycle, the total heat released was almost the same as in the fast cycle. Figure 18b compares the peak heat release rate of each particle and the CAD it occurred in the fast and slow cycles. The peak heat release rates reached by particles in the faster burning cycle were higher than the slow cycle. This was because the rate of heat release was lower in the individual particles in the slow cycle due to the lower temperature of the entrained zone. After 40 CAD ATDC the peak heat release rates dropped off in the slow cycle due to expansion reducing the temperature. The particles

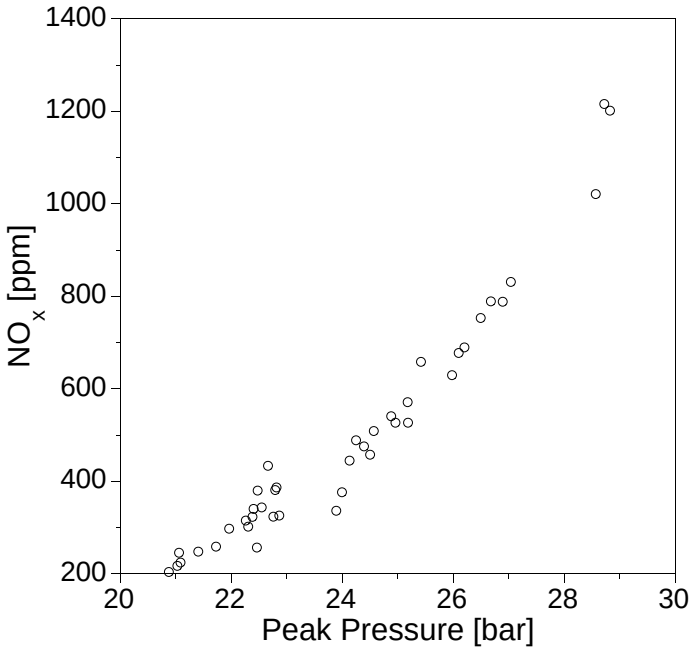

Figure 16: *NO_x emissions against the peak pressure during the cycle they occurred in 40 simulated cycles.*

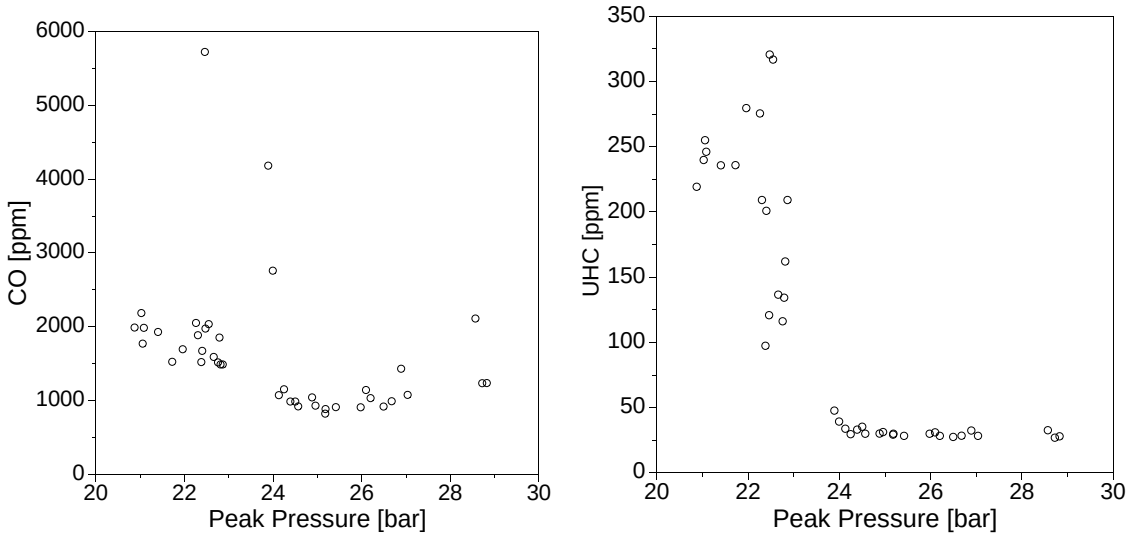

Figure 17: *CO and UHC emissions against the peak pressure during the cycle they occurred in 40 simulated cycles.*

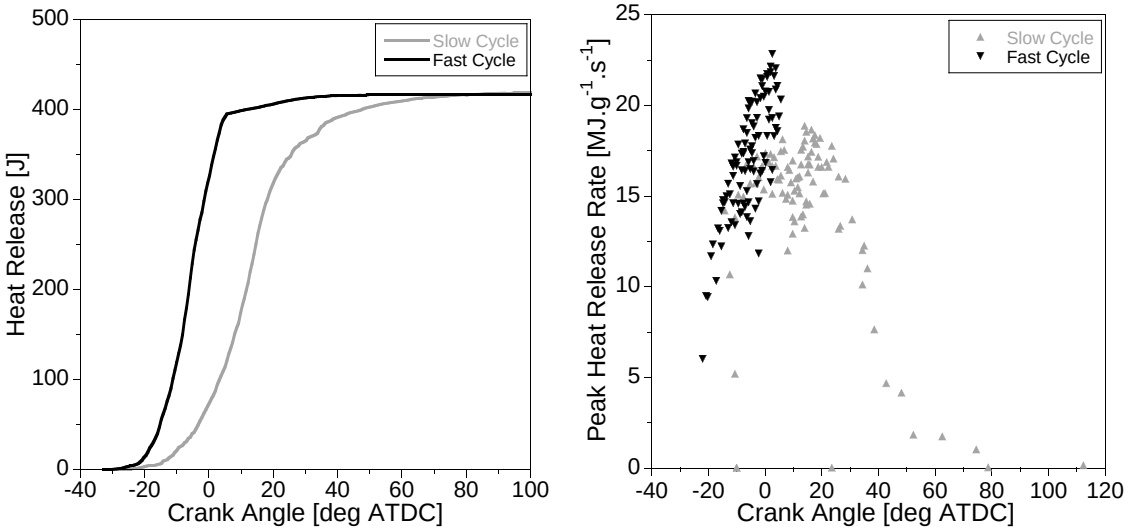

(a) (b)

Figure 18: *Heat released in the fast and slow cycles and the peak heat release rate in each particle against the CAD at which they occurred.*

Table 6: *HCCI operating condition.*

Speed [RPM]	1510
BMEP [bar]	2.62
Fuel mass/cyl./cyc. [mg]	9.8
IVO [CAD BTDC]	295
IVC [CAD BTDC]	125
EVO [CAD ATDC]	109
EVC [CAD ATDC]	279
Main inj. [CAD BTDC]	260
Pilot inj. [CAD ATDC]	315

with the lower peak heat release rates were the main source of UHC.

3.4 Effect of SI EGR on HCCI

The SI-HCCI engine was also used to calibrate the SRM in HCCI mode. The engine was operated with NVO, trapping roughly 50 % of the cylinder charge. A dual injection strategy was used where 20 % of the fuel was injected during NVO, referred to as pilot injection, and the remainder close to IVO. The HCCI operating condition is given in Table 6.

The main combustion and NVO were simulated with the SRM and the breathing events

were simulated in GT-Power. Figure 19a shows the average pressure profiles during the main combustion over 40 simulated and 200 experimental cycles. The average simulated profile matches experimental data well. The NVO pressure profiles are compared in Figure 19b and suggest the simulated heat release during NVO is slightly lower and occurs later than in the experiment. Peak pressures against the crank angle they occurred for forty consecutive cycles are compared with experimental results in Figure 20. Simulated peak pressures occur slightly earlier than in the experiment. The average fuel air equivalence ratio obtained in the simulation was 1.25, compared with a measured value of 1.33. This value is important as a poor match would suggest incorrect EGR mass and temperatures at EVC and IVC. Emissions data is given in Table 7. More details on the HCCI engine simulation will be presented elsewhere.

Table 7: *Emission results for SI-HCCI engine in HCCI mode.*

	Exp.	Sim.
NO_x [ppm]	15	8
CO [ppm]	1032	13
UHC [ppm]	2958	9

The model contains a crevice but no wall impingement sub-model, which could be one cause of the low CO and UHC emissions obtained in the simulation. The under prediction could also be due to the assumption that the cylinder charge was homogeneous at IVC. The UHC emissions should not have had a direct impact on the following combustion due to the fuel injected during NVO, however the heat released during NVO may have been effected.

The effect of exhaust gas compositions from different SI cycles on HCCI combustion was investigated. The exhaust gas composition from the fast, medium and slow cycles shown in Figure 12 were used in NVO simulations, without fuel injection, and the IVO compositions were stored. An exhaust gas containing only a mixture of water, carbon dioxide and nitrogen that would result from complete stoichiometric combustion of the fuel was also created. The resulting detailed IVO compositions and the stoichiometric EGR were then used in identical HCCI combustion events making up 51 % of the charge. The EGR mass during the transition would be lower due to the higher exhaust temperatures in SI mode and the shorter NVO duration at the start of the switch between operating modes. This study was however aimed at investigating the effect of compositions from different SI cycles.

Figure 21 shows the fast burn cycle's EGR caused a misfire and the slow burn cycle's EGR caused an advanced combustion phasing compared with the medium burn's exhaust composition. The results show the stoichiometric EGR created will not be sufficient for simulating the transition. To achieve a stable transition it is necessary to investigate the effect of different SI cycles as different compositions were found to cause very different HCCI combustion events. Figure 16 showed the variation in NO_x between SI cycles was

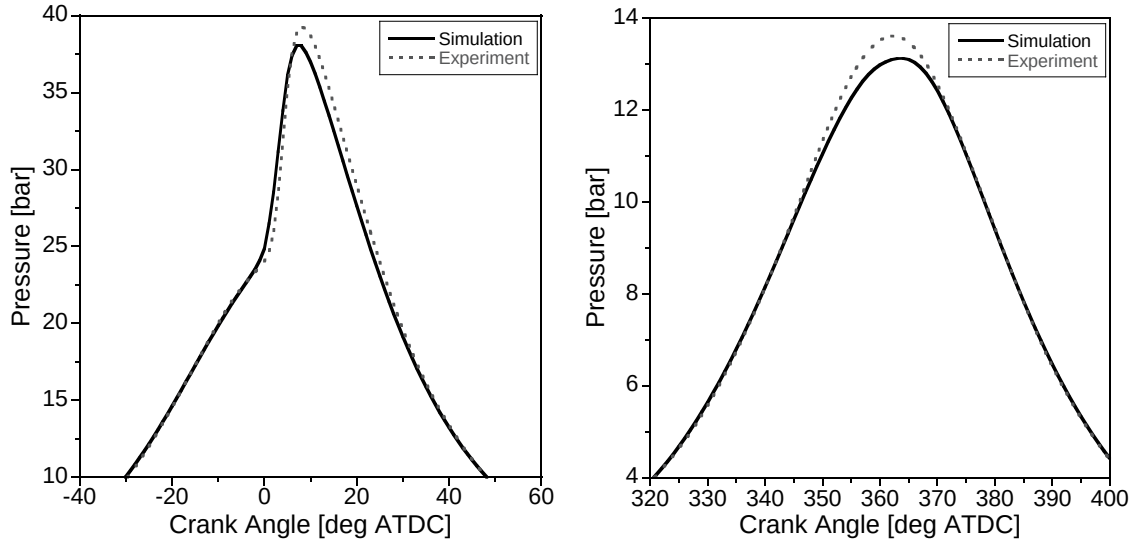

Figure 19: *Average pressure profiles of 40 simulated and 200 experimental HCCI cycles during (a) main combustion and (b) NVO.*

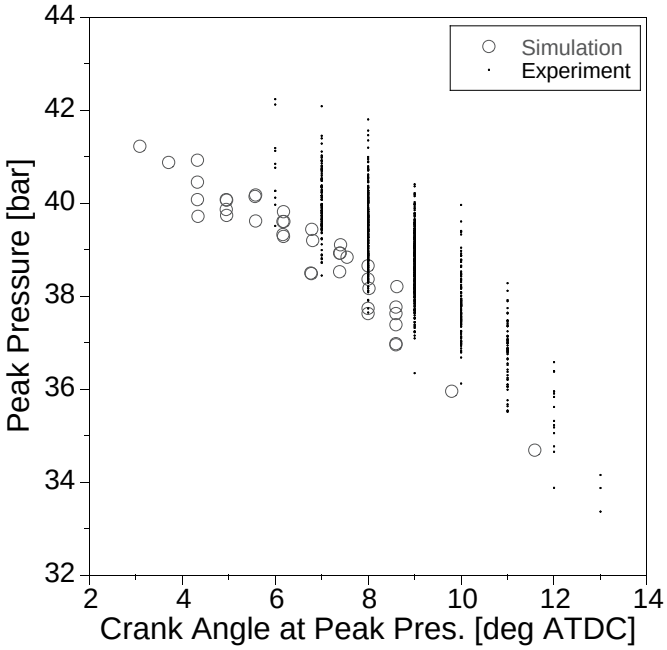

Figure 20: *Peak pressure against the crank angle it occurs for 40 simulated and 200 experimental HCCI cycles.*

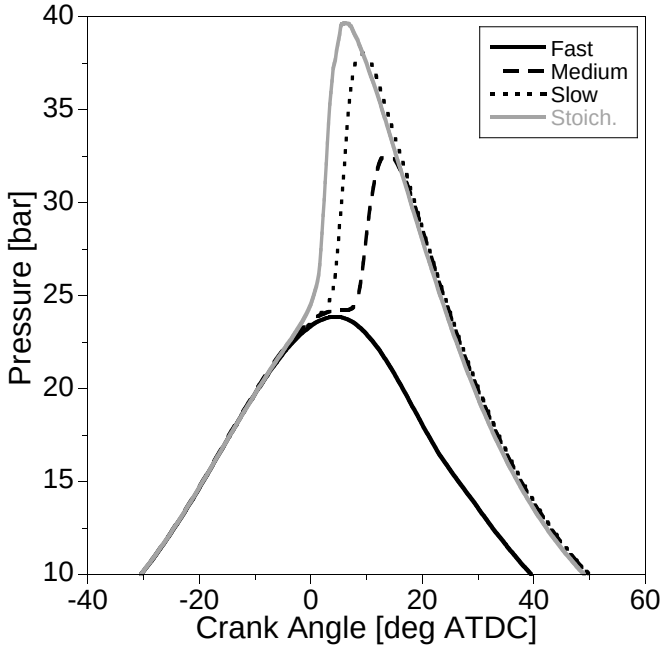

Figure 21: *Pressure traces from HCCI combustion using EGR from fast medium and slow SI cycles and a stoichiometric EGR.*

large. NO_x is known to advance HCCI combustion phasing at low concentrations [30] and then to retard the phasing when the concentration is increased further. NO_x emissions are extremely dependent on the temperature history in the cylinder and the reactions involving NO_x cannot be assumed to reach equilibrium behind the flame front. The model presented here was able to predict NO_x emissions well which was an important result if it is to be used for simulating the transition in a detailed chemistry HCCI model.

4 Conclusions

A new PDF based Stochastic Reactor Model for simulating spark ignition engines has been developed. The particle ensemble was split into unburned, entrained and burned zones. Mixing occurred within each zone but not between zones. A detailed mechanism was used to perform chemistry in each of the zones resulting in an exhaust gas composing of 157 species.

Experimental results from a single cylinder research engine that showed low CCV were compared with the simulation. Key parameters in the calibrated model were then investigated. The temperature used at the spark did not affect the simulation results at the conditions studied. The size of the initial flame kernel also had low impact on the simulation over a wide range of values suggesting the spark initiation sub-model was sufficient.

Experiments on a four-cylinder SI engine resulted in cycle to cycle fluctuations. The new SI model was coupled with GT-Power to enable multi-cycle simulation of the four-cylinder engine. The variation of peak pressures and crank angles they occurred matched experimental data well. The average NO_x emissions also matched the experiment suggesting correct combustion temperatures in the model.

The engine can also operate in HCCI mode by switching the cam profiles and injection strategy. The SRM was calibrated in HCCI mode and the effect on HCCI combustion of the detailed exhaust gas composition from SI cycles was investigated. The exhaust gas composition from a fast, medium and slow SI cycle were used in identical HCCI simulations. EGR from slower SI cycles was found to advance HCCI combustion due to a chemical effect.

The model will be used to simulate the switch between SI-HCCI-SI operating modes in future work, with the aim of improving the stability of the transition. It may be necessary to reduce CCV at the relevant SI speeds and loads before a smooth transition can be obtained. Trends between peak cylinder pressure and emissions were observed. Measuring individual cylinder pressures in the final cycle before HCCI could be necessary for achieving the best possible transition.

Acknowledgement

Funding from the EPSRC (UK), grant number EP/D068703/1, is gratefully acknowledged. Experimental data has been provided by the Internal Combustion Engine Group, University of Oxford.

List of Symbols and Abbreviations

Symbols

C_1	Entrainment rate constant	[-]
CAD_{spark}	Spark timing angle	[CAD ATDC]
HRR_{lim}	Heat release rate limit	[MJ.kg^{-1}.s^{-1}]
l_T	Characteristic length scale	[m]
N_B	Number of burned particles	[-]
N_E	Number of entrained particles	[-]
N_U	Number of unburned particles	[-]
N_{Tot}	Total number of particles at IVC	[-]
P_{max}	Peak pressure	[bar]
$R_{f;n}$	Flame radius at nth CAD step	[m]
S_L	Laminar flame speed	[m.s^{-1}]
t	Time after IVC	[s]
t_{spark}	Spark time	[s]
t_{stop}	Time at EVO	[s]
Δt	Time step	[s]
t_E^{max}	Maximum entrained time	[s]
$\bar{u}_i$	Mean inlet gas speed	[m.s^{-1}]
u_T	Characteristic flame speed	[m.s^{-1}]
V^B	Burned zone volume	[m^3]
V^E	Entrained zone volume	[m^3]
V_f	Flame volume calculated from the radius	[m^3]
V_{next}^U	Volume of the next particle to be entrained	[m^3]
ρ_i	Inlet air density	[kg.m^{-3}]
ρ_u	Unburned zone density	[kg.m^{-3}]
τ_b	Characteristic burn time	[s]
τ_E	Entrained zone mixing time	[s]
τ_E^{max}	Maximum entrained zone mixing time	[s]

Abbreviations

ATDC	After top dead centre
BTDC	Before top dead centre
CAD	Crank angle degree
CCV	Cycle to cycle variation
CFD	Computational fluid dynamics
CIDI	Compression ignition direct injection
CPU	Central processing unit
CR	Compression ratio
EGR	Exhaust gas recycle
EMST	Euclidean minimum spanning tree
EVC	Exhaust valve close
EVO	Exhaust valve open
HCCI	Homogeneous charge compression ignition
IVC	Inlet valve close
IVO	Inlet valve open
NVO	Negative valve overlap
PDF	Probability density function
PRF	Primary reference fuel
RON	Research octane number
SI	Spark ignition
SRM	Stochastic reactor model
TDC	Top dead centre
UHC	Unburned hydrocarbons

References

[1] M. Kraft, P. Maigaard, F. Mauss, M. Christensen, and B. Johansson. Investigation of combustion emissions in a homogeneous charge compression injection engine: Measurements and a new computational model. *Proceedings of the Combustion Institute*, 28:1195–1201, 2000.

[2] A. Fuerhaptor, W. Piock, and G. Fraidl. CSI - Controlled Auto Ignition the Best Solution for the Fuel Consumption Versus Emission Trade-Off? SAE Paper No. 2003-01-0754, 2003.

[3] A. Fuerhaptor, E. Unger, W. Piock, and G. Fraidl. The new AVL CSI Engine - HCCI Operation on a Multi Cylinder Gasoline Engine. SAE Paper No. 2004-01-0551, 2004.

[4] L. Koopmans and I. Denbratt. A Four Stroke Camless Engine, Operated in Homogeneous Charge Compression Ignition Mode with Commercial Gasoline. SAE Paper No. 2001-01-3610, 2001.

[5] L. Koopmans, O. Backlund, and I. Denbratt. Cycle to Cycle Variations: Their Influence on Cycle Resolved Gas Temperature and Unburned Hydrocarbons from a Camless Gasoline Compression Ignition Engine. SAE Paper No. 2002-01-0110, 2002.

[6] L. Koopmans, H. Strom, S. Lundgren, O. Backlund, and I. Denbratt. Demonstrating a SI-HCCI-SI Mode Change on a Volvo 5-Cylinder Electronic Valve Control Engine. SAE Paper No. 2003-01-0753, 2003.

[7] A. Kulzer, J. Hathout, C. Sauer, R. Karrelmeyer, W. Fischer, and A. Christ. Multi-Mode Combustion Strategies with CAI for a GDI Engine. SAE Paper No. 2007-01-0214, 2007.

[8] G. Tian, Z. Wang, Q. Ge, J. Wang, and S. Shuai. Mode Switch of SI-HCCI Combustion on a GDI Engine. SAE Paper No. 2007-01-0195, 2007.

[9] R. Wagner, K. Edwards, C. Daw, J. Green Jr., and B. Bunting. On the Nature of Cyclic Dispersion in Spark Assisted HCCI Combustion. SAE Paper No. 2006-01-0418, 2006.

[10] C.S. Daw, R.M. Wagner, K.D. Edwards, and J.B. Green Jr. Understanding the transition between conventional spark-ignited combustion and HCCI in a gasoline engine. *Proceedings of the Combustion Institute*, 31:2887–2894, 2007.

[11] J. Ewald and N. Peters. On unsteady premixed turbulent burning velocity prediction in internal combustion engines. *Proceedings of the Combustion Institute*, 31:3051–3058, 2007.

[12] Z. Tan and R. D. Reitz. An ignition and combustion model based on the level-set method for spark ignition engine multidimensional modeling. *Combustion and Flame*, 145:1–15, 2006.

[13] H. Bayraktar. Theoretical investigation of flame propagation process in an SI engine running on gasoline-ethanol blends. *Renewable Energy*, 32:758–771, 2007.

[14] M. Baratta, A. Catania, E. Spessa, and A. Vassallo. Development and Assessment of a Multizone Combustion Simulation Code for SI Engines Based on a Novel Fractal Model. SAE Paper No. 2006-01-0048, 2006.

[15] E. Abdi Aghdam, A. Burluka, T. Hattrell, K. Liu, C. Sheppard, J. Neumeister, and N. Crundwell. Study of Cyclic Variation in an SI Engine Using Quasi-Dimensional Combustion Model. SAE Paper No. 2007-01-0939, 2007.

[16] J. Serras-Pereira, P. Aleiferis, D. Richardson, and S. Wallace. Mixture Preparation and Combustion Variability in a Spray-Guided DISI Engine. SAE Paper No. 2007-01-4033, 2007.

[17] A. Brown, C. Stone, and P. Beckwith. Cycle-by-Cycle Variations in Spark Ignition Engine Combustion - Part I Flame Speed and Combustion Measurements and a Simplified Turbulent Combustion Model. SAE Paper No. 960612, 1996.

[18] C. Stone, A. Brown, and P. Beckwith. Cycle-by-Cycle Variations in Spark Ignition Engine Combustion - Part II Modelling of Flame Kernel Displacements as a Cause of Cycle-by-Cycle Variations. SAE Paper No. 960613, 1996.

[19] H. Daneshyar and P. G. Hill. The structure of small-scale turbulence and its effect on combustion in spark ignition engines. *Prog. Energy Combust. Sci.*, 13:47–73, 1987.

[20] H. Su, A. Vikhansky, S. Mosbach, M. Kraft, A. Bhave, K. Kim, T. Kobayashi, and F. Mauss. A computational study of an HCCI engine with direct injection during gas exchange. *Combustion and Flame*, 147:118–132, 2006.

[21] A. Bhave, M. Kraft, L. Montorsi, and F. Mauss. Sources of CO emissions in an HCCI engine: A numerical analysis. *Combustion and Flame*, 144:634–637, 2006.

[22] S. Mosbach, A. Aldawood, and M. Kraft. Real-Time Evaluation of a Detailed Chemistry HCCI Engine Model Using a Tabulation Technique. *Combustion Science and Technology*, 180:1263–1277, 2008.

[23] S. Subramaniam and S. B. Pope. A Mixing Model for Turbulent Reactive Flows based on Euclidean Minimum Spanning Trees. *Combustion and Flame*, 115:487–514, 1998.

[24] A. Gogan, A. Lehtiniemi, F. Mauss, and B. Sundén. Stochastic Reactor Model for Auto Ignition Calculation in Spark Ignition Engine. Proceedings of the European Combustion Meeting 2005, 2005.

[25] A. Gogan, B. Sundén, A. Lehtiniemi, and F. Mauss. Stochastic Model for the Investigation of the Influence of Turbulent Mixing on Engine Knock. SAE Paper No. 2004-01-2999, 2004.

[26] J. B. Heywood. *Internal Combustion Engine Fundamentals*. McGraw-Hill, New York, 1988.

[27] J. Tagalian and J. Heywood. Flame Initiation in a Spark-Ignition Engine. *Combust. Flame*, 64:243–246, 1986.

[28] J. Keck. Turbulent flame structure and speed in spark-ignition engines. *Nineteenth Symposium (International) on Combustion/The Combustion Institute*, pages 1451–1466, 1982.

[29] S. Karagiorgis, N. Collings, K. Glover, N. Coghlan, and A. Petridis. Residual Gas Fraction and Estimation on a Homogeneous Charge Compression Ignition Engine Utilizing the Negative Valve Overlap Strategy. SAE Paper No. 2006-01-3276, 2006.

[30] P. Risberg, G. Kalghatgi, H. Ångström, and F. Wahlin. Auto-ignition quality of Diesel-like fuels in HCCI engines. SAE Paper No. 2005-01-2127, 2005.